frontiers in Astronomy and Space Sciences

ORIGINAL RESEARCH
published: 12 June 2020
doi: 10.3389/fspas.2020.00018

Ultraviolet Photoprocessing of Glycine Adsorbed on Various Space-Relevant Minerals

Giovanni Poggiali[1,2], *Teresa Fornaro*[2], *Simone Potenti*[3], *Maria Angela Corazzi*[1,2] *and John Robert Brucato*[2]*

[1] Deparment of Physics and Astronomy, University of Florence, Florence, Italy, [2] INAF-Astrophysical Observatory of Arcetri, Florence, Italy, [3] Scuola Normale Superiore, Pisa, Italy

The discovery of amino acids such as glycine on meteorites and comets confirms the role of small bodies as transport and delivery vehicles of building blocks of life on Earth and possibly on other planetary bodies of our Solar System. Glycine is quite interesting because it is the simplest of the 20 biogenic amino acids, from which complex organic molecules might have originated in our evolved Solar System. To investigate the possible chemical evolution of this molecule in space, it is important to consider how the interaction with mineral matrices influences its photostability. Indeed, the presence of minerals can mediate the effects of electromagnetic radiation, catalyzing photoreactions, or protecting molecules against degradation. Such interactions are responsible for the preservation/degradation mechanisms of organic molecules in space environments. Laboratory simulations of UV processing may provide key insights into the survival of organic molecules in space environment and rocky surfaces, which is of particular relevance for current missions of sample return from asteroids, such as NASA OSIRIS-REx and JAXA Hayabusa 2, and in particular, upcoming space exploration missions on planetary surfaces, such as ESA-Roscosmos ExoMars 2022 and NASA Mars 2020. In this article, we report a laboratory study of UV irradiation of glycine adsorbed on various space relevant minerals: forsterite, antigorite, spinel, and pyrite. We monitored possible changes of glycine functional groups due to UV irradiation through *in situ* infrared (IR) spectroscopic analysis. Results show that degradation of glycine occurs with a half-life of 0.5–2 h depending on the mineral substrate. Appearance of new IR bands suggests the occurrence of catalytic reactions mediated by minerals and UV.

Keywords: astrobiology, biomarker, glycine, laboratory, UV irradiation

OPEN ACCESS

Edited by:
Isik Kanik,
NASA Jet Propulsion Laboratory (JPL), United States

Reviewed by:
María-Paz Zorzano,
Centro de Astrobiología (CSIC-INTA), Spain
Felipe Gómez,
Centro de Astrobiología (CSIC-INTA), Spain

***Correspondence:**
John Robert Brucato
john.brucato@inaf.it

Specialty section:
This article was submitted to Astrobiology, a section of the journal Frontiers in Astronomy and Space Sciences

Received: *31 January 2020*
Accepted: *17 April 2020*
Published: *12 June 2020*

Citation:
Poggiali G, Fornaro T, Potenti S, Corazzi MA and Brucato JR (2020) Ultraviolet Photoprocessing of Glycine Adsorbed on Various Space-Relevant Minerals. Front. Astron. Space Sci. 7:18. doi: 10.3389/fspas.2020.00018

INTRODUCTION

Interactions at the interfaces between minerals and prebiotic molecules and their role in the origin of life are some of the most discussed topics in astrobiology (Bernal, 1951; Luther et al., 1998; Ertem, 2004; Hazen and Sverjensky, 2010; Lambert et al., 2017). Several processes can be involved in surface-promoted reactions: e.g., ion exchange, electron transfer reactions, photolysis, photocatalysis, and photosynthesis (Schoonen et al., 2004). Even before the formation of the rocky surfaces of planets, asteroids, and other minor bodies, mineral surfaces of dust grains in the interstellar medium may promote the synthesis of complex molecules (Brucato et al., 2006).

Moreover, the discovery of organic molecules on asteroids and comets confirmed the role of small bodies as transport and delivery vehicles of building blocks of life on Earth and possibly on other bodies of the Solar System (Rivkin and Emery, 2010). Therefore, it is extremely important to study the role of mineral–molecule interactions on the chemical evolution of organic molecules in space and their fate once they are delivered on planetary surfaces. Rocky surfaces are irradiated by solar UV photons and cosmic rays and are constantly subjected to thermal changes determined by their rotation and orbit. However, we know that UV photons can penetrate only a few millimeters in regolith (Muñoz Caro et al., 2006). Thus, in the absence of resurfacing processes, organics in the near subsurface are shielded. Nevertheless, UV-driven chemical reactions between molecules and the surface can cause the formation of very reactive species acting as strong oxidants that can penetrate deeper in the subsurface and degrade organic matter. Furthermore, the results reported in this work show that a few hours of exposure to UV may transform organic molecules during their absorption phase on a mineral substrate, and if subsequent deposition of a shielding material occurs, such as dust grains or ices accumulating in deep space or sediments on a planet, these molecules would be preserved in an altered state. Therefore, studies on photoprocessing and survivability of prebiotic molecules on rocky surfaces are fundamental both to understand their role in the origin of life and to estimate the likelihood of preservation of possible biomarkers that might be detected in such conditions by space missions.

Among all the molecules detected in space, the amino acid glycine (H_2NCH_2COOH) [from now GLY using the standard abbreviation] is particularly interesting. It is the simplest amino acid and one of the 20 ordinary amino acids, or proteinogenic amino acids, incorporated biosynthetically into proteins during translation. In solution and solid phase GLY exists mainly as zwitterion ($^+H_3NCH_2COO^-$) (Rosado et al., 1998). Zwitterion is the electrically neutral form of a molecule that has both positive and negative charges localized. Amino acids, in which a basic amine group ($–NH_2$) acts as a proton acceptor from a carboxylic acid group (–COOH) that acts as proton donor, form zwitterionic species as a consequence of an internal acid–base reaction. In the astrophysical context, GLY plays an important role; along with other amino acids, it was found incorporated in meteorites (Kvenvolden et al., 1970) and seems to be the only amino acid that can survive, sublimating from the surface of a meteorite during atmospheric entry of a meteoroid (Glavin and Bada, 2004). This amino acid was recently detected by the ROSINA instrument on board the Rosetta spacecraft in the coma of comet 67P/Churyumov-Gerasimenko (Altwegg et al., 2016; Hadraoui et al., 2019), confirming the results of the Stardust mission on the presence of complex organic molecules in cometary material (Glavin et al., 2008). However, despite many attempts, it was not observed in submillimetric observations of interstellar medium and star formation regions (Snyder et al., 2005).

To investigate the survivability of GLY in space environments, laboratory studies are an unavoidable step toward a comprehensive understanding of its fate. Although many studies have been conducted so far to investigate UV processing of amino acids, and in particular GLY, only few studies investigated the stability of such molecules in presence of minerals. Almost 20 years have passed since the first studies on the formation of GLY within astrophysical ices analogs were conducted, both experimentally (Bernstein et al., 2002; Muñoz Caro et al., 2002) and theoretically (Woon, 2002; Holtom et al., 2005). At the same time, studies on the stability of GLY were carried out in the simplest way possible: sublimation of the amino acids on a substrate window and then either UV irradiation or ion bombardment of the sample, recording mostly infrared (IR) spectra in transmission. A summary of previous experiments of UV irradiation of GLY and half-life is reported in **Table 1**. Regarding the study of GLY stability, it is worth mentioning the exposure experiment of GLY carried out in space. A thin solid film of GLY, both pure and mixed with montmorillonite clays, was exposed to solar UV irradiation with the BIOPAN-2 system devised by ESA fixed to the exterior of a Russian FOTON-11 descent capsule for 10 days (solar light received 37,428 W m^{-2}) (Barbier et al., 2002). Post-flight free amino acids were derivatized and analyzed by reverse-phase high performance liquid chromatography (HPLC). Results showed that 66% of the original GLY amount (53% in the presence of mineral) remained unaltered, confirming the data obtained during previous missions (Barbier et al., 1998). Then a new photochemistry experiment called UVolution was performed (Guan et al., 2010) as part of the payload of the BIOPAN-6 space facility on board Russian satellite FOTON M3 and supported by laboratory analog analysis. A thin GLY film with a thickness of a few hundred nm was exposed during the mission to a flux of 29 solar constant hours in the 220–280 nm range. In first-order kinetic analysis by degradation of IR bands, the authors evaluated a photodestruction rate of $1 \cdot 10^{-6}\ s^{-1}$ corresponding to a half-life of 8 days for GLY at 1 AU. Samples prepared in the same conditions were irradiated in laboratory for 6 h by microwave-powered H_2/He-flow lamp (flux $8 \cdot 10^{14}$ photons $s^{-1}cm^{-2}$) and the results show a photodestruction rate of $8 \cdot 10^{-6}\ s^{-1}$ corresponding to a half-life of 1 day. More recently, in the PROCESS experiment of the European EXPOSE-E exposure facility on the European Space Agency (ESA)'s Columbus module of ISS, GLY was deposited as a homogeneous thin film on a quartz window and exposed for 1.5 yr (Noblet et al., 2012). At the end of the exposure time all the samples were totally destroyed and the GLY half-life was 8 h.

Several other experiments were conducted on the stability of GLY to other types of irradiation (X-ray or ion bombardment simulating cosmic rays) but, although they have considerable importance in the general framework of understanding the survival of GLY in various space environments, they are not mentioned here because they cannot be directly compared with our results.

In recent years, some researchers have started to investigate the role of minerals in the stability of GLY, and other amino acids, with particular relevance for the upcoming *in situ* exploration missions on planetary surfaces such as ESA-Roscosmos ExoMars 2022 (Vago et al., 2015) and NASA Mars 2020 (Williford et al., 2018). Some experiments investigated the effect of adsorption of GLY on minerals without irradiation.

TABLE 1 | Recap on literature irradiation experiments with GLY deposited on windows.

Reference	Sample	Irradiation setup	Half-life in laboratory	Extrapolation in space
Ehrenfreund et al. (2001) Confirmed by Peeters et al. (2003)	GLY deposited on CsI window mixed with Ar, N_2 or H_2O ices at 12 K to simulate interstellar environment	Microwave-excited hydrogen flow lamp, flux $1 \cdot 10^{15}$photons $s^{-1}cm^{-2}$ between 110 and 185 nm	700–1,000 s	320 yr and $32 \cdot 10^6$ yr in interstellar medium
ten Kate et al. (2005)	GLY deposited on silicon disc	Hydrogen flow lamp, flux $4.6 \cdot 10^{14}$photons $s^{-1}cm^{-2}$ between 120 and 180 nm	4,300 s	22 h and in order of 10^7 yr when embedded in regolith in Mars context
		Deuterium discharge lamp, flux $4.9 \cdot 10^{13}$ photons $s^{-1}cm^{-2}$ between190 and 400 nm	$1.8 \cdot 10^6$ s	
Poch et al. (2013, 2014)	300 nm, GLY deposit on a magnesium fluoride (MgF_2) window	Xenon arc lamp, flux $5.570.3 \cdot 10^{19}$ photons $s^{-1}m^{-2}$ in range 200–300 nm at 218 K and pressure 6 mbar	About 300 h (depending on sample thickness)	In Mars context estimation not included
Orzechowska et al. (2007)	GLY in water ice films sublimated and frozen in ∼mm-thick layer on an OFHC copper substrate	Argon mini-arc lamp, flux of $1.2 \cdot 10^{14}$photons $s^{-1}m^{-2}$ between 130 and 335 nm at 100 K	50–3.7 h	About 10 yr scaled at Europa
Johnson et al. (2012)	GLY is sublimated in Ar matrix on KBr window at 18 K	Monochromatic resonance line lamps: Xe lamp at 147 nm, I2 lamp at 206 nm and a Hg pen-ray lamp at 254 nm ($1.09 \cdot 10^{19}$ at 147 nm, $8.68 \cdot 10^{18}$ at 206 nm and $3.41 \cdot 10^{18}$ photons $s^{-1}cm^{-2}$ at 254 nm)	30 min with Xe, 50 min with I_2, and 700 min with Hg lamp	160–5 yr scaled at Europa

The table shows a selection of previous experiments on GLY irradiated with UV lamps. The first column reports the reference of experiments, the second and third columns summarize, respectively, sample preparation and irradiation setup, and fourth and fifth columns display reported results and extrapolation to space environment (if available).

Galvez-Martinez et al. (2019) sublimated and subsequently adsorbed GLY on pyrite crystals under ultra-high vacuum (UHV) conditions to study possible surface effects. Interesting results were observed using *in situ* XPS. Specifically, the NH_3^+ peak showed a decrease in intensity with increasing time (from 58 to 35%), indicating that the pyrite surface caused a transition process from a zwitterionic to an anionic species over time on the monosulfide-enriched surface. Moving to UV irradiation experiments, dos Santos et al. (2016) analyzed in the laboratory the survival of GLY spiked on a large set of Martian-like minerals. The samples were irradiated with a xenon (Xe) light source for 28 h in a simulated Martian atmosphere with a thermal cycle −80°C/+20°C of 2 h. All the samples were extracted from minerals and analyzed post-irradiation with gas chromatography–mass spectrometry. Experiments with different concentrations of GLY in a spiked solution showed that minerals such as smectite clays (montmorillonite, nontronite, and saponite), sulfates (gypsum and jarosite), and olivine (forsterite) better preserve amino acids, while augite, basaltic lava, enstatite, and hematite are less efficient in preserving amino acids. Regarding the pyrite mineral, de La Cruz-López et al. (2017) investigated its influence in stabilizing GLY against UV irradiation. In their experiment, the amino acid was spiked on pyrite and irradiated with a mercury lamp (with a primary energy being 254 nm, 5.5 Wm^{-2}) for a period from 1 up to 24 h. Authors concluded that glycine irradiated in the UV showed no clear changes, which is consistent with the chemical stability of glycine against exposure to ionizing radiation.

In our laboratory simulations we chose various minerals from different groups to simulate space environments and in particular Mars. Phyllosilicates were observed on Mars (Carter et al., 2009), indicating the occurrence of aqueous alteration in early Mars history. Among phyllosilicates, we used antigorite, $[Mg, Fe]_3Si2O_5(OH)_4$, which is one of the three common forms of serpentine. It is a hydrated silicate (with structural water or hydroxyl groups) and in natural form it has a lamellar appearance with well-defined cleavages. Serpentines draw attention in the context of the origin of life because they are products of serpentinization, probably one of the most relevant processes in hydrothermal vents (Bach et al., 2006). Serpentines were also found on Mars (Ehlmann et al., 2009, 2010, 2011; Viviano-Beck et al., 2014). Within the neosilicate group we selected forsterite Mg_2SiO_4, which is the magnesium-rich end-member of the olivine group. It is a representative of mafic minerals and one of the most abundant silicate minerals on rocky bodies (Steel, 1989; Messenger et al., 2005; Brownlee et al., 2006; Chevrier and Mathé, 2007; Weinbruch et al., 2010; Poteet et al., 2011). Forsterite is also one of the minerals

involved in the geological process of serpentinization, which is then converted into serpentine. These two minerals were used in a previous work performed in our laboratory (Fornaro et al., 2018a), and further discussion on their relevance can be found there.

In addition, we studied interaction of GLY with spinel, $MgAl_2O_4$. Spinel-group minerals are found in a wide range of terrestrial and extratrrestrial geological environments (Bjärnborg and Schmitz, 2013). Spinel was found in Martian meteorite SaU008 (Yu and Gee, 2005). The last mineral of our set was pyrite, FeS_2, an iron sulfide found on Mars as small grains (Moriarty et al., 2010) and in Martian meteorites (Agee et al., 2013).

MATERIALS AND METHODS

Sample Preparation

A 99% sample of glycine was purchased from Merk/Sigma-Aldrich (catalog no. G6388). Antigorite (from Złoty Stok, Poland) was purchased from Nuova Didattica, forsterite and spinel (from Vesuvio, Italy) were purchased from Webminerals s.a.s., and pyrite (from Cerro de Pasco, Peru) was purchased from a private geologist.

Natural minerals were ground with Retsch Planetary Ball Mill PM100 (agate jar and spheres) and subsequently selected in grain size 20–50 μm by Retsch Vibratory Sieve Shaker AS200. Clearing of organic contaminants on minerals was performed by washing with methanol and ultrapurified water ddH2O (18.5 MΩ) through sonication and ultrasonic bath. Forsterite was further treated through oxidation of organics with hydrogen peroxide in a solution of 30% (w/w) because it still showed organic contaminants after washing with methanol. IR spectroscopy characterization of mineral after the treatments showed the absence of bands linked with organic contaminants. These kinds of treatments were used effectively in previous work carried out by our laboratory group (Fornaro et al., 2013a,b). The motivation to apply this grinding is to simulate the powdered surface of planets and other rocky bodies. Moreover, powdered mineral samples also allow maximization of molecule–mineral interactions, as well as molecular diffusion inside the mineral matrix. Specifically, smaller mineral grain size corresponds to higher surface area available for molecular interactions.

An incipient wetness impregnation technique (spiking) was used for rapid adsorption of a controlled number of molecules on solid mineral grains. First, we estimated in a separate experiment the impregnation ratio defined as the adsorbed volume of solvent at incipient wetness per mineral powder mass unit. We performed this measurement adding ultrapure water to the support mineral until separate liquid phase was observed. Measured values of impregnation ratio are reported in **Table 2**. We used 300 mg of each mineral and 15 mg of GLY molecule with a molecule/mineral ratio 1:20. Stock solutions with ddH2O were prepared in Eppendorf tubes, and then they were spiked onto mineral samples. Afterwards, samples were vortex-mixed to homogenize the suspensions and then dried in an oven at 50°C for 12 h. In this way, we prepared samples of GLY adsorbed on four minerals: antigorite, forsterite, spinel and pyrite, with grain dimensions ranging from 20 to 50 μm.

TABLE 2 | Impregnation ratio estimated values for four mineral samples.

Mineral	Impregnation ratio [μL/μg]	Solvent [μL]
Antigorite	0.4	120
Forsterite	0.4	120
Pyrite	0.4	120
Spinel	0.5	150

Irradiation Setup and IR Analysis

The UV source used in our experiments is a Newport Xe-enhanced UV 300 W lamp with purified Xe at 5–20 bar (wavelength range 185–2,000 nm) (Newport, 2020). Xe arc lamps have a relatively smooth emission curve in the UV–VIS spectrum, with sun-like emission spectrum and 5800 K color temperature. The Xe lamp is hosted in Newport Research Arc Lamp Housing 50–500 W. The UV radiation emitted by the lamp was collimated through an optical system consisting of a first mirror that reflects the radiation coming from the lamp to a UV-grade fused silica collimating condenser lens (type Fused Silica Asphere, f-number f/2.2), which directs collimated UV radiation toward an optical fiber with an aperture of 800 μm. The optical fiber was inserted into the sample chamber of the interferometer, located at an angle of 60° with respect to the sample. The area of the irradiated sample, A_0, was 7.07 mm^2. The sample holder was 4 mm thick with a total volume of V = 0.03 mL. The lamp was calibrated at the National Institute of Optics (INO) in Arcetri (Firenze, Italy); the total incident flux of UV photons focused on the samples through the optical fiber per area unit was $\frac{\Phi_{tot}}{A_0} = 1.05 \cdot 10^{17}$ photons s^{-1} cm^{-2} calculated in the range 200–350 nm where GLY absorption is higher (Saidel et al., 1952; Ehrenfreund et al., 2001). This range was confirmed in our work collecting UV spectra of water–GLY solution with different concentrations using ONDA UV-30 SCAN (UV/Vis) photospectrometer, as shown in **Figure 1**. We cannot exclude that a minor fraction of VIS radiation could be absorbed by minerals (in particular those containing iron) and used to induce photocatalytic processes.

IR analysis was carried out with a Bruker VERTEX 70v interferometer interfaced with Harrick Praying Mantis™ for DRIFTS analysis. Spectra were acquired in the wavenumber range from 8,000 to 400 cm^{-1} with resolution of 2 cm^{-1}. OPUS software was used to perform our analysis; we used the basic algorithms available in the software to evaluate band areas and peak position. Spectroscopic analysis of photodissociation process was performed during irradiation without moving the samples and saturating the Praying Mantis™ with nitrogen atmosphere in order to rule out any oxidation due to air at room temperature (25°C). IR diffuse reflectance spectra of the samples were recorded at regular intervals of UV irradiation time in order to monitor the degradation process in real time by observing changes in the IR spectrum features. From recorded spectra, degradation kinetics was investigated and the rate of band intensity reduction was evaluated. In particular, we calculated band areas assuming their proportionality to the number of molecules. The degradation rate β was obtained by fitting the

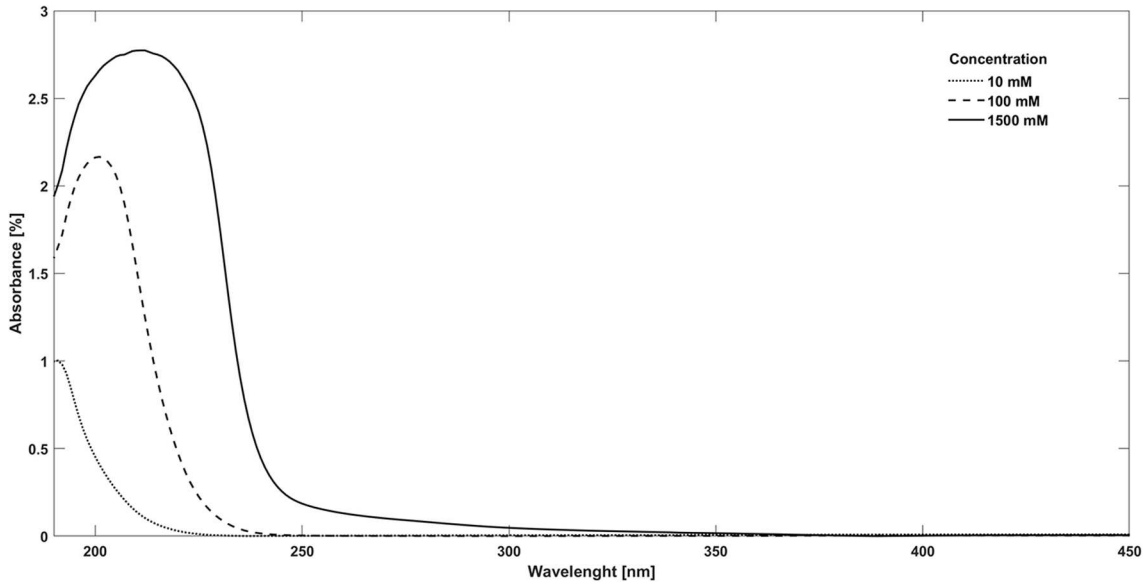

FIGURE 1 | Water–glycine adsorption UV spectra at various concentrations: dotted line, 10 mM; dashed line, 100 mM; and continuous line, 1,500 mM.

fraction of unaltered molecules, $N_{(t)}/\ N_0$, estimated by the band area at irradiation time t normalized on the band area pre-irradiation, vs. time, using an exponential function:

$$\frac{N(t)}{N_0} = Be^{-\beta t} + C$$

where N_0 is the initial number of molecules in the sample, B is the fraction of molecules that interact with UV radiation, and C is the fraction of molecules that do not interact with UV radiation due to their position in deep layers of the solid samples. From the degradation rate we can obtain the half-life (time required to destroy 50% of the initial material) as $t_{1/2} = \ln(2/\beta)$, and the UV destruction cross section σ, which represents the probability of interaction between UV radiation and the adsorbed molecule. For the cross section, the relation with β is

$$\beta = \sigma \frac{\Phi_{\text{tot}}}{A_0}$$

During the irradiation of GLY adsorbed on pyrite, we observed the formation of new bands. In this case, we investigated the kinetics through the function

$$N_f(t) = N_{f_0}\left(1 - e^{-\alpha t}\right)$$

where $N_f(t)$ is the number of molecules formed at time t, N_{f_0} is the maximum number of molecules formed, and α is the formation rate. Similarly to the previous case, this function gives best fits for band formation processes. In this case, the cross section of the formation process σ_f is linked to α by the relation

$$\alpha = \sigma_f \frac{\Phi_{\text{tot}}}{A_0}$$

More details on the methods used for analyzing the degradation kinetics can be found in previous works (Fornaro et al., 2013b, 2018a; Potenti et al., 2018).

RESULTS

Band Assignment and Spectral Changes Due to Molecular Adsorption

Peak assignments of pure GLY spectrum based on experimental and theoretical data from the literature (Holtom et al., 2005; Pilling et al., 2013) are reported in the first two columns of **Table 3**. We focused our analysis of the IR spectrum of GLY on the range 3,800–400 cm^{-1}, because the spectrum of pure solid GLY shows 15 identified vibrational modes in this range (assignments are shown in **Figure 2**), while above 3,800 cm^{-1} unidentified absorption peaks are present. We noted that vibrational modes are distributed within two distinct main regions: one from 1,900 to 400 cm^{-1} characterized by vibrational modes of carboxylate $-COO^-$ and a second one, at higher wavenumbers (shorter wavelengths), due to very weak vibrational modes such as the stretching bands of the protonated amine group NH_3^+. The full-range spectrum of pure GLY is reported in **Supplementary Figure A1**. The presence of modes of the NH_3^+ functional group, such as its asymmetric stretching at ∼3,200 cm^{-1}, and carboxylate modes, such as symmetric stretching at ∼1,400 cm^{-1}, confirms that GLY in solid phase is mainly in the zwitterionic form.

An example of how spectral features can change before and after GLY adsorption is reported in **Figure 3** for pyrite, where spectra of pure GLY, pure pyrite, and GLY adsorbed on pyrite are shown. The spectra before and after adsorption for all the samples are reported in **Supplementary Figures A2–A5**. Our peak assignment for GLY adsorbed on mineral samples is

TABLE 3 | Band assignment for pure GLY and GLY adsorbed on minerals.

Mode	Peak position (cm^1)									
	Pure GLY		GLY on forst.		GLY on pyr.		GLY on spin.		GLY on antig.	
	Peak	Int.	Peak	Int.	Peak	Int.	Peak	Int.	Peak	Int.
ωCOO^-	614	w	n.o.	—	614	w	n.o.	—	n.o.	—
δCOO^-	713	w	n.o.	—	705	w	n.o.	—	n.o.	—
νCC	884 901	w	n.o.	—	866 895	w	n.o.	—	n.o.	—
ϱCH_2	920	m	n.o.	—	916	m	n.o.	—	n.o.	—
νCN	1,038	w	n.o.	—	n.o.	—	n.o.	—	n.o.	—
ϱNH_3^+	1,120 1,136	w	1,130	w	1,120 1,136	vw	n.o.	—	1,118 1,134	w
$twCH_2$	1,315	vw	1,311	W	1,310	w	1,313	w	1,312	w
ωCH_2	1,336	m	1,335	s	1,337	m	1,333	m	1,333	w
$\nu_s COO^-$	1,400 1,419	m	1,393 1,413	s	1,418	w	1,392 1,411	m	1,391 1,412	w
δCH_2	1,444	w	1,444	w	n.o.	—	1,443	w	1,444	w
δNH_3^+	1,503 1,535	s	1,501 1,523	m	1,498 1,522	w	1,503 1,530	m	1,503 1,513 1,530	w
$\nu_{as} COO^-$	1,610 1,640	vs	1,601	s	1,605 1,661	w	1,585 1,611	w	n.o.	—
$\nu NH_3^+ + \tau NH_3^+$	2,130	vw	2,134	m	2,127	w	2,118	w	2,116	W
$\nu NH_3^+ + \nu CN$	2,654	vw	2,615	w	2,615	w	2,620	w	2,621	*W*
$\nu_{as} NH_3^+$	3,200	vw	3,177	m	3,178	w	3,165	m	3,169	M

Vibrational modes: ν, stretching; δ, bending; ω, wagging; ρ, rocking; τ, torsion; tw, twisting; s, symmetric; as, asymmetric. Band intensities: vw, very weak <1%; w, weak 1–4%; m, medium 4–8%; s, strong 8–10%; vs, very strong >10%. Several unidentified combination bands were observed between 2,000 and 3,000 cm^{-1}. [n.o. stands for "not observed"].

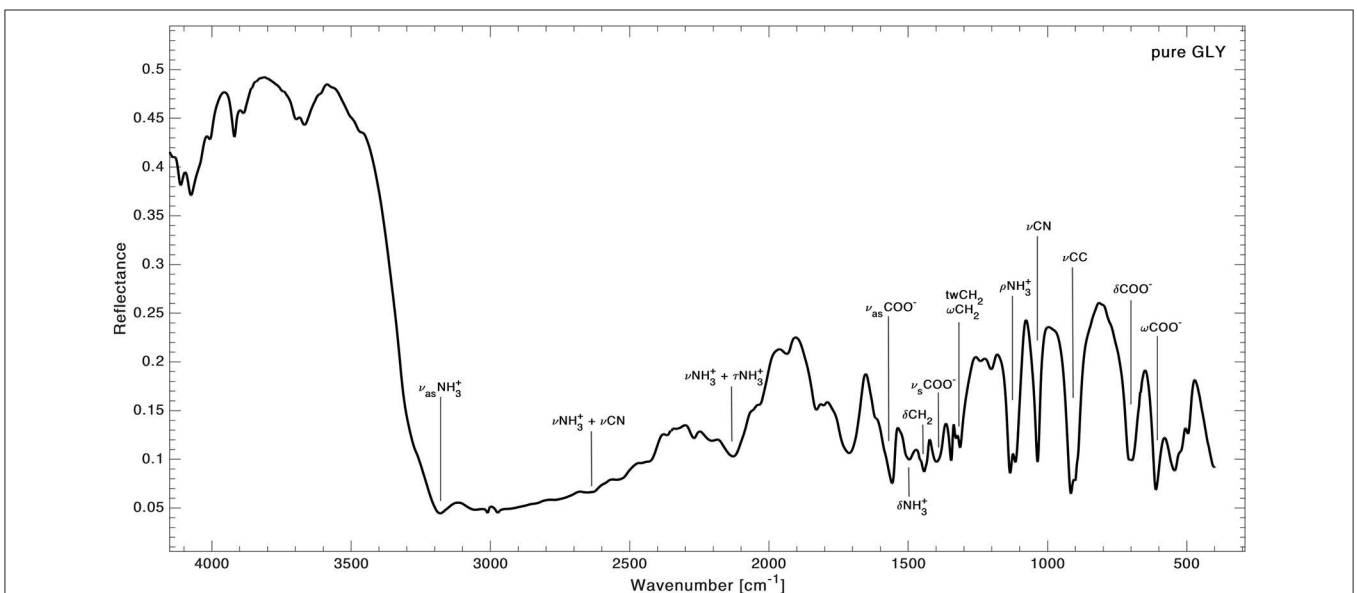

FIGURE 2 | Infrared spectrum of pure GLY in the range 4,000–400 cm^{-1} with peaks assignment from Holtom et al. (2005) and Pilling et al. (2013). Vibrational modes legend: ν, stretching; δ, bending; ω, wagging; ρ, rocking; τ, torsion; *tw*, twisting; *s*, symmetric; *as*, asymmetric.

reported in the last four columns of **Table 3** with relative band intensities. As it is possible to notice, a number of vibrational modes of pure GLY are missing when GLY is adsorbed on mineral surfaces, with the lowest number of bands observed in the case of spinel and antigorite (nine peaks). Interestingly, some of the characteristic bands of pure GLY disappear, especially in

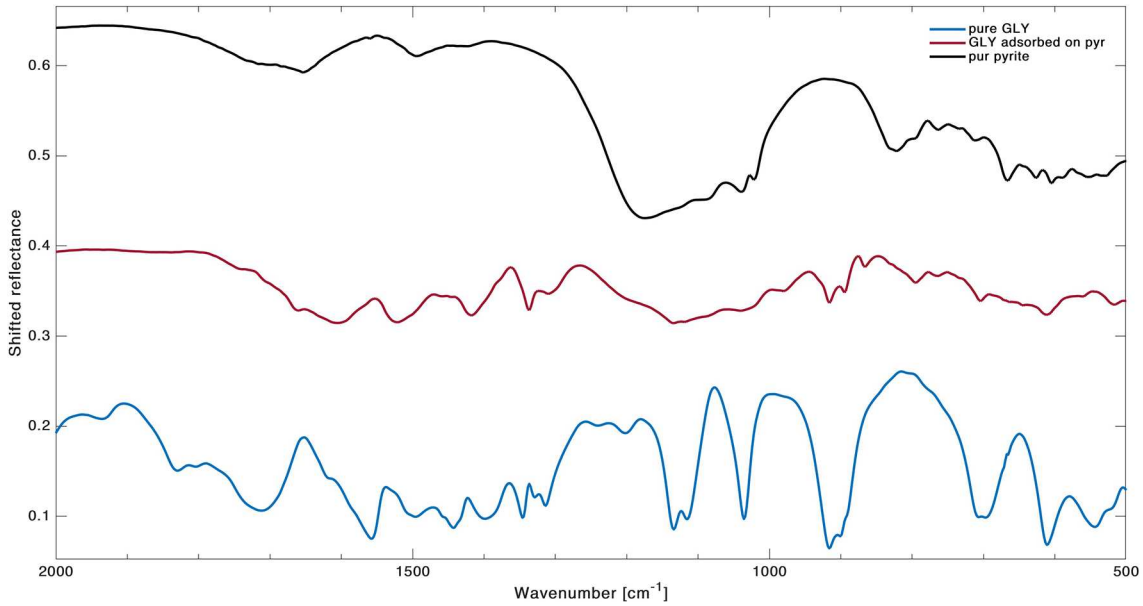

FIGURE 3 | Detail of spectra in wavenumber range 2,000–500 cm^{-1} with comparison between pure GLY (blue line), pure pyrite (black line, shifted 0.3 to the top), and GLY adsorbed on pyrite (red line, shifted 0.15 to the top).

TABLE 4 | Best-fit values for the degradation rate β, cross section σ_{lab}, and half-life time $t_{1/2lab}$ for pure GLY irradiated in laboratory conditions.

Mode	β [min^{-1}]	σ_{lab} [cm^2]	$t_{\frac{1}{2}}$ [min]
NH_3^+ group domain: 3,400–1,900 cm^{-1}	no degradation		
COO^- group I domain: 1,900–810 cm^{-1}	$2.033 \cdot 10^{-4}$	$(1.94 \pm 0.04) \cdot 10^{-21}$	3, 409
COO^- group II domain: 810–470 cm^{-1}	$3.724 \cdot 10^{-4}$	$(3.55 \pm 0.07) \cdot 10^{-21}$	1, 861

Analysis was conducted on three different spectral domains.

the spectrum region under 1,000 cm^{-1} where mineral features are predominant. On the contrary, some peaks become more distinguishable in the region 3,500–2,000 cm^{-1}. In the case of GLY adsorbed on forsterite some bands become stronger. Moreover, we observed that peak positions of GLY adsorbed on mineral surfaces are not the same for all samples. All the spectra show two regions characterized by GLY bands: a series of weak overlapping bands extending from 3,300 to 2,000 cm^{-1}, corresponding mainly to the NH, CH, or CN stretching vibrations or some combination bands, and another region of more intense bands from 1,600 to 1,300 cm^{-1}, which are bending spectral signatures of $-COO^-$, C–H, and $-NH_3^+$. In detail, the only sample showing molecular bands under 1,000 cm^{-1} is GLY adsorbed on pyrite. Here we observed shifts of about 4–18 cm^{-1} toward smaller wavenumbers in almost all bands; the higher shift of 18 cm^{-1} was observed for the stretching mode of *CC*, indicating some interactions of GLY with pyrite through the *CC* group. The wagging mode of COO^- at 614 cm^{-1} is the only unmodified GLY peak in this spectral region. In the spectral region 1,600 to 1,300 cm^{-1} we observed GLY bands in almost all the samples with the exception of NH_3^+ rocking mode missing on spinel and CH_2 bending mode missing on pyrite. In this spectral range, shifts are smaller compared to lower wavenumbers and some bands do not change position at all, such as the NH_3^+ rocking mode and CH_2 bending mode. Symmetric stretching of COO^-, which in pure GLY is present as a peak and a shoulder at 1,400/1,419 cm^{-1}, shifts toward smaller wavenumbers in all the samples, with shifts of 7/4 cm^{-1} in the case of forsterite, 8/8 cm^{-1} in the case of spinel and 9/7 cm^{-1} in the case of antigorite. This indicates that the carboxylate functional group of GLY interacts with the mineral surface sites in all cases. On pyrite, such band has only one peak at 1,418 cm^{-1}. Also, the asymmetric stretching of COO^-, located at 1,610/1,640 cm^{-1} pure GLY, shifts in position in almost all samples with the exception of antigorite. At higher wavenumber, between 3,500 and 2,000 cm^{-1}, we observed several bands related to the combination mode of NH_3^+. Here the intensity of bands increases after the adsorption and all the peaks shift toward smaller wavenumber. For asymmetric stretching of NH_3^+, located at 3,200 cm^{-1} in pure GLY, we observed a shift of about 30 cm^{-1} toward smaller wavenumbers when GLY is adsorbed on minerals, with the bigger shift of 35 cm^{-1} in the case of spinel and the smaller shift of 22 cm^{-1} in the case of pyrite.

Irradiation Experiments

Pure GLY powder was ground using a mortar and pestle and placed directly in the sample holder. Sample irradiation occurred under a nitrogen atmosphere for 7–8 h at room temperature, recording IR spectra at intervals of 1 h. No changes in band intensities were observed, so we tried a long irradiation for 61.5 h

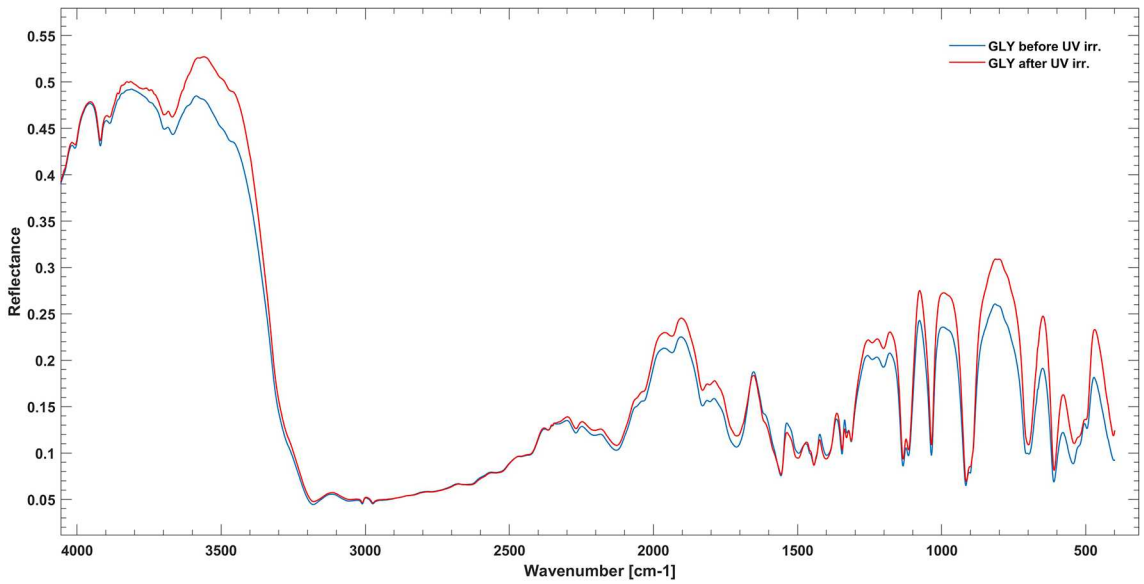

FIGURE 4 | Infrared spectrum of pure GLY in the range 4,000–400 cm^{-1} before (blue line) and after (red line) 61.5 h of UV irradiation.

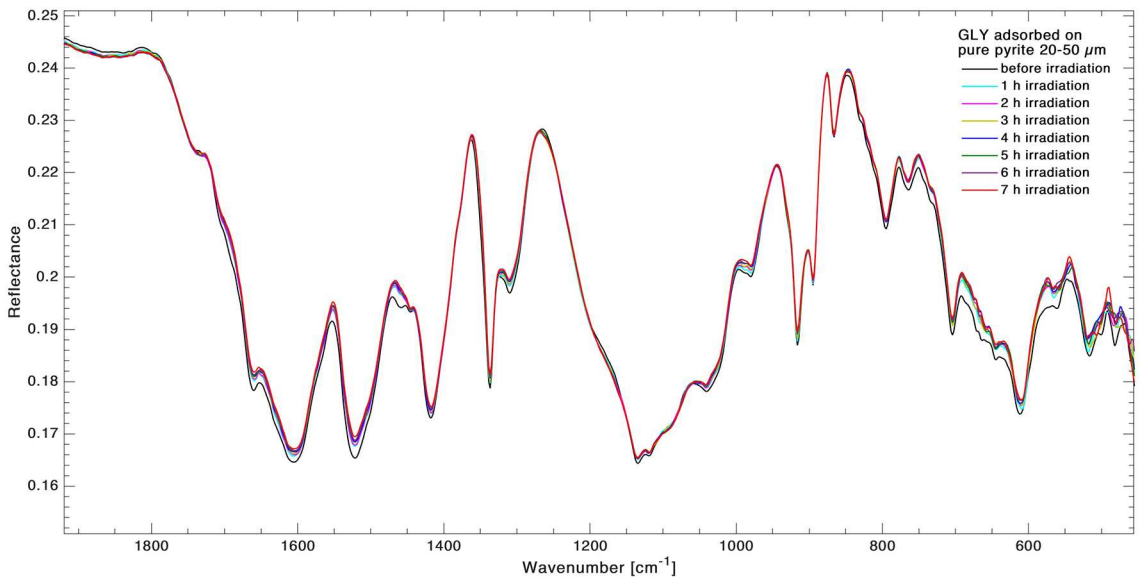

FIGURE 5 | Superimposition of infrared spectra of GLY adsorbed on pyrite in the range 2,000–500 cm^{-1} during 7 h of UV irradiation. Spectra were collected *in situ* at 1-h intervals to monitor the kinetics of degradation in real time.

at room temperature. In this case, we collected only the final spectrum, and we noticed some weak changes by comparison with the pre-irradiation spectrum. To estimate degradation parameters, we used a more simplified equation for degradation kinetics: $\ln\left[\frac{N(t)}{N_0}\right] \propto -\beta t$. This formula is more suitable for integration on extended domains [a similar procedure is used in Guan et al. (2010)]. Results on degradation rates, cross sections, and half-life are reported in **Table 4**, while spectra before and after UV irradiation are shown in **Figure 4**. As reported, pure GLY shows half-life of the order of a few days in laboratory conditions.

UV photodissociation analysis was then performed on GLY adsorbed on four minerals: antigorite, forsterite, spinel and pyrite. In such cases, after a total time of 7 h of irradiation in laboratory conditions (room temperature under nitrogen flux) for each sample, several GLY bands showed non-negligible degradation. In **Figure 5** we report the spectra at subsequent irradiation times for GLY adsorbed on pyrite in the range

TABLE 5 | Best-fit values of the degradation rate β, the fraction of molecules that interact with UV radiation *B*, and the fraction of molecules that do not interact with UV radiation *C*, for GLY adsorbed on minerals UV irradiated in laboratory conditions.

Peak [cm^{-1}]	Mode	β [min^{-1}]	*B*	*C*	χ^2_{dof}
GLY adsorbed on forsterite					
1,130	ρNH_3^+	0.037 ± 0.011	0.080 ± 0.002	0.920 ± 0.002	0.965
1,311 and 1,335	$twCH_2$ and ωCH_2	0.015 ± 0.002	0.118 ± 0.004	0.882 ± 0.004	0.965
1,393–1,413	$\nu_s COO^-$	0.012 ± 0.002	0.135 ± 0.005	0.865 ± 0.005	0.958
1,444	δCH_2	0.02 ± 0.011	0.11 ± 0.01	0.89 ± 0.01	0.742
1,501–1,523	δNH_3^+	0.028 ± 0.018	0.054 ± 0.005	0.946 ± 0.005	0.747
1,601	$\nu_{as} COO^-$	0.0061 ± 0.0013	0.12 ± 0.01	0.88 ± 0.01	0.949
2,134	$\nu NH_3^+ + \tau NH_3^+$	0.031 ± 0.010	0.078 ± 0.002	0.922 ± 0.002	0.940
2,615	$\nu NH_3^+ + \nu CN$	0.023 ± 0.008	0.081 ± 0.004	0.919 ± 0.004	0.895
3,177	$\nu_{as} NH_3^+$		d.n.e.		
GLY adsorbed on antigorite					
1,118–1,134	ρNH_3^+		d.n.e.		
1,312 and 1,333	$twCH_2$ and ωCH_2	0.0104 ± 0.0014	0.071 ± 0.003	0.929 ± 0.003	0.977
1,391–1,412	$\nu_s COO^-$	0.014 ± 0.004	0.097 ± 0.006	0.903 ± 0.006	0.904
1,444	δCH_2		d.n.e.		
1,503–1,513–1,530	δNH_3^+	0.006 ± 0.004	0.078 ± 0.017	0.922 ± 0.017	0.749
2,116	$\nu NH_3^+ + \tau NH_3^+$		d.n.e.		
2,621	$\nu NH_3^+ + \nu CN$	0.005 ± 0.003	0.034 ± 0.009	0.966 ± 0.009	0.843
3,169	$\nu_{as} NH_3^+$		No degradation		
GLY adsorbed on spinel					
1,313 and 1,333	$twCH_2$ and ωCH_2	0.0047 ± 0.0016	0.029 ± 0.005	0.971 ± 0.005	0.938
1,392–1,411	$\nu_s COO^-$	0.0053 ± 0.0014	0.027 ± 0.003	0.973 ± 0.003	0.956
1,443	δCH_2		d.n.e.		
1,503–1,530	δNH_3^+	0.009 ± 0.002	0.031 ± 0.002	0.969 ± 0.002	0.925
1,585–1,611	$\nu_{as} COO^-$		No degradation		
2,118	$\nu NH_3^+ + \tau NH_3^+$		d.n.e.		
2,620	$\nu NH_3^+ + \nu CN$		No degradation		
3,165	$\nu_{as} NH_3^+$		No degradation		
GLY adsorbed on pyrite					
614	ωCOO^-		No degradation		
705	δCOO^-		No degradation		
866–895	νCC	0.007 ± 0.004	0.060 ± 0.013	0.940 ± 0.013	0.758
916	ρCH_2	0.006 ± 0.002	0.099 ± 0.012	0.901 ± 0.012	0.923
1,120–1,136	ρNH_3^+	0.0017 ± 0.0012	0.22 ± 0.12	0.78 ± 0.12	0.967
1,310	$twCH_2$	0.021 ± 0.002	0.142 ± 0.009	0.858 ± 0.009	0.988
1,337	ωCH_2	0.0187 ± 0.0019	0.158 ± 0.003	0.842 ± 0.003	0.989
1,418	$\nu_s COO^-$	0.009 ± 0.004	0.056 ± 0.006	0.944 ± 0.006	0.846
1,498–1,522	δNH_3^+	0.047 ± 0.0017	0.064 ± 0.011	0.936 ± 0.011	0.934
1,605–1,661	$\nu_{as} COO^-$		d.n.e.		
2,127	$\nu NH_3^+ + \tau NH_3^+$	0.008 ± 0.002	0.097 ± 0.009	0.902 ± 0.009	0.987
2,615	$\nu NH_3^+ + \nu CN$		No degradation		
3,178	$\nu_{as} NH_3^+$		No degradation		

Except pyrite, $twCH_2$ and ωCH_2 were evaluated together due to band overlapping. d.n.e. stands for "degradation not evaluable" when samples showed degradation but analysis was not possible. In the χ^2_{dof} column is reported the chi square evaluated for the fitting procedure.

2,000–500 cm^{-1}. Best fit values for β, B, and C for single bands in all the samples are reported in **Table 5**. The destruction cross sections and half-life derived from photodissociation parameters are reported in **Table 6**. We noted a generic cross section decrease at increasing wavenumber (shorter wavelength). Some minerals do not show band reduction at higher wavelength, and the degradation seems to be more intense within the region 1,100–1,300 cm^{-1}, as inferred by photodissociation parameters and cross section values. Some differences were observed among minerals, with some minerals having generally lower degradation

TABLE 6 | Destruction cross sections σ_{lab} and half-life $t_{1/2\ lab}$ in laboratory conditions for single bands of GLY adsorbed on minerals under UV irradiation.

Peak [cm^{-1}]	Mode	$\sigma_{lab}[cm^2]$	$t_{1/2\ lab}[min]$
GLY adsorbed on forsterite			
1,130	ρNH_3^+	$(3.5 \pm 1.1) \cdot 10^{-19}$	18 ± 5
1,311 and 1,335	$twCH_2$ and ωCH_2	$(1.4 \pm 0.2) \cdot 10^{-19}$	47 ± 6
1,393–1,413	$\nu_s COO^-$	$(1.1 \pm 0.2) \cdot 10^{-19}$	58 ± 9
1,444	δCH_2	$(1.9 \pm 1.0) \cdot 10^{-19}$	34 ± 19
1,501–1,523	δNH_3^+	$(2.6 \pm 1.7) \cdot 10^{-19}$	25 ± 16
1,601	$\nu_{as} COO^-$	$(5.8 \pm 1.3) \cdot 10^{-20}$	113 ± 24
2,134	$\nu NH_3^+ + \tau NH_3^+$	$(2.9 \pm 1.0) \cdot 10^{-19}$	22 ± 7
2,615	$\nu NH_3^+ + \nu CN$	$(2.2 \pm 0.8) \cdot 10^{-19}$	30 ± 10
GLY adsorbed on antigorite			
1,312 and 1,333	$twCH_2$ and ωCH_2	$(9.9 \pm 1.5) \cdot 10^{-20}$	67 ± 9
1,391–1,412	$\nu_{as} COO^-$	$(1.4 \pm 0.4) \cdot 10^{-19}$	46 ± 12
1,503–1,513–1,530	δNH_3^+	$(6 \pm 4) \cdot 10^{-20}$	109 ± 68
2,621	$\nu NH_3^+ + \nu CN$	$(5 \pm 3) \cdot 10^{-20}$	136 ± 80
GLY adsorbed on spinel			
1,313 and 1,333	$twCH_2$ and ωCH_2	$(4.5 \pm 1.6) \cdot 10^{-20}$	146 ± 49
1,392–1,411	$\nu_s COO^-$	$(15.1 \pm 1.4) \cdot 10^{-20}$	130 ± 34
1,503–1,530	δNH_3^+	$(8 \pm 2) \cdot 10^{-20}$	78 ± 18
GLY adsorbed on pyrite			
866–895	νCC	$(7 \pm 4) \cdot 10^{-20}$	99 ± 57
916	ρCH_2	$(6 \pm 2) \cdot 10^{-20}$	106 ± 33
1,120–1,136	ρNH_3^+	$(1.6 \pm 1.2) \cdot 10^{-20}$	405 ± 284
1,310	$twCH_2$	$(2.1 \pm 0.2) \cdot 10^{-19}$	32 ± 3
1,337	ωCH_2	$(1.8 \pm 0.2) \cdot 10^{-19}$	37 ± 4
1,418	$\nu_s COO^-$	$(9 \pm 4) \cdot 10^{-20}$	73 ± 30
1,498–1,522	δNH_3^+	$(5 \pm 2) \cdot 10^{-20}$	147 ± 53
2,127	$\nu NH_3^+ + \tau NH_3^+$	$(8 \pm 2) \cdot 10^{-20}$	86 ± 21

Pyrite, $twCH_2$, and ωCH_2 were evaluated together due to band overlapping. Cross sections and half-life in table are reported only for bands where photodissociation parameters were evaluated.

rates. This is reflected in half-life values as can be seen in **Table 6**. We found almost an order of magnitude difference among minerals. Similar to the case of pure GLY, we evaluated also degradation parameters and derivate values for extended spectral domain, generally encompassing a domain in the region dominated by NH_3^+ bands and one or two domains in the region dominated by $-COO^-$ and C–H bands, according to spectral features. Results are reported in **Tables 7**, **8**.

During irradiation of pyrite, we observed the formation of new bands, as shown in **Figure 6**; a new band, related to CO_2, appeared at 2,340 cm^{-1}. Some modifications of spectral shape were also observed in the region 2,500–2,400 cm^{-1}. The best fit values for CO_2 band formed at 2,340 cm^{-1} are: formation rate $\alpha = 0.0176 \pm 0.0019$ min^{-1} and formation cross sections $\sigma_f = (1.7 \pm 0.2) \cdot 10^{-19} cm^2$.

DISCUSSION

In this work, we investigated the UV photodestruction process of GLY, either pure or adsorbed on minerals, by monitoring the disappearance in the IR spectrum of some characteristic signals related to the main amino acid functional groups during irradiation. The photodestruction rate constants obtained in this study can be used to predict amino acid survival in different extraterrestrial environments.

We found that, in our laboratory conditions, pure GLY has a half-life of 1–2 days, consistent with the findings of Guan et al. (2010), although in other simulated space conditions it seems to be less photostable, with a reported half-life time of 700–1,000 s in Ehrenfreund et al. (2001). This result is therefore consistent with the chemical stability of GLY against exposure to ionizing radiation, in agreement with previous works also with other types of radiation (de La Cruz-López et al., 2017). However, we have to consider the possibility that glycine features do not show significant changes in band intensities because DRIFT spectroscopy involves a sample layer much thicker than the one affected by UV irradiation. As a consequence, any possible changes occurring at the very outermost GLY monolayers could be too small to be detected because the spectrum arising from the UV-unaffected deeper layers could predominate.

In the case of GLY adsorbed on minerals, before the irradiation experiment, we observed a different spectroscopic behavior as a consequence of molecular adsorption onto minerals, as reported in **Table 3** and in the Results section. The observed changes, such as band disappearance and frequency shifts, are linked to different adsorption configurations of GLY on the selected minerals. In our samples we observed that (1) the GLY bands are missing in particular below 1,000 cm^{-1} in all samples except pyrite; (2) some other bands are missing at higher wavenumbers; and (3) the lowest number of bands is observed on spinel and antigorite. Disappearance of molecular features or their changes in intensity could be related to molecular spatial arrangements as imposed by surface selection rules (Fornaro et al., 2013a). Shifts of vibrational frequencies due to molecule–mineral interactions were also observed in all cases. Shifts of band peak position of molecular functional groups to higher wavenumber values can be interpreted as a strengthening of the chemical bonds of these functional groups due to molecular adsorption; on the other hand, a shift toward lower wavenumber values indicates a weakening of the chemical bonds of these functional groups as a consequence of interactions with mineral surface sites.

It is worth noting that the observation of such shifts in peak position of GLY adsorbed on different mineral phases is an essential piece of information for spectroscopic matching of data acquired from IR instruments on board space missions. Referring to spectra of pure minerals and molecules in the process of feature identification can lead to misinterpretation if the possible shifts in peak positions due to molecule–mineral interactions are not considered. Analysis of samples obtained with physical adsorption processes under plausible space-like conditions is fundamental to support present and future space missions in the search for organic matter and biomarkers in the Solar System.

We expected also that the differences in molecule–mineral interactions, coupled with the different catalytic properties of the minerals, could lead to UV irradiation specificity. We observed degradation in all GLY-mineral samples during 7 h of irradiation. The degradation generally seems to be more intense around

TABLE 7 | Best-fit values of the degradation rate β, the fraction of molecules that interact with UV radiation B, and the fraction of molecules that do not interact with UV radiation *C*, for spectral domains of GLY adsorbed on minerals UV irradiated in laboratory conditions.

Spectral domains [cm^{-1}]	β [min^{-1}]	B	C	χ^2_{dof}
GLY adsorbed on forsterite				
NH_3^+ group domain: 3,396–2,302		d.n.e.		
COO^- group domain: 1,983–1,280	0.022 ± 0.004	0.090 ± 0.002	0.910 ± 0.002	0.969
GLY adsorbed on antigorite				
NH_3^+ group domain: 3,340–2,298	0.005 ± 0.002	0.044 ± 0.009	0.956 ± 0.009	0.918
COO^- group domain: 1,925–1,050	0.017 ± 0.007	0.0116 ± 0.009	0.9884 ± 0.009	0.829
GLY adsorbed on spinel				
NH_3^+ group domain: 3,425–2,298		No degradation		
COO^- group domain: 1,900–1,080		d.n.e.		
GLY adsorbed on pyrite				
NH_3^+ group domain: 3,440–2,367		No degradation		
COO^- group I domain: 1,800–1,268	0.012 ± 0.003	0.056 ± 0.003	0.943 ± 0.003	0.942
COO^- group II domain: 1,267–875	0.005 ± 0.002	0.016 ± 0.003	0.983 ± 0.003	0.982

d.n.e. stands for "degradation not evaluable" when samples showed degradation but analysis was not possible. In the χ^2_{dof} column is reported the chi square evaluated for the fitting procedure.

TABLE 8 | Destruction cross sections σ_{lab} and half-life $t_{1/2\ lab}$ in laboratory conditions for spectral domains of GLY adsorbed on minerals under UV irradiation.

Spectral domain [cm^{-1}]	σ_{lab} [cm^2]	$t_{1/2\ lab}$[min]
GLY adsorbed on forsterite		
NH_3^+ group domain: 3,396–2,302	d.n.e.	
COO^- group domain: 1,983–1,280	$(2.1 \pm 0.4) \cdot 10^{-19}$	32 ± 5
GLY adsorbed on antigorite		
NH_3^+ group domain: 3,340–2,298	$(4 \pm 2) \cdot 10^{-20}$	145 ± 60
COO^- group domain: 1,925–1,050	$(1.6 \pm 0.7) \cdot 10^{-19}$	41 ± 17
GLY adsorbed on spinel		
NH_3^+ group domain: 3,425–2,298	No degradation	
COO^- group domain: 1,900–1,080	d.n.e.	
GLY adsorbed on pyrite		
NH_3^+ group domain: 3,440–2,367	No degradation	
COO^- group I domain: 1,800–1,268	$(1.1 \pm 0.3) \cdot 10^{-19}$	56 ± 13
COO^- group II domain: 1,267–875	$(5 \pm 2) \cdot 10^{-20}$	135 ± 53

d.n.e. stands for "degradation not evaluable" when samples showed degradation but analysis was not possible.

the region 1,300–1,500 cm^{-1}, which is characterized by spectral signatures of $-CH_2-$ and $-COO^-$. This trend confirms previous studies that localize mostly UV irradiation effects on the carboxyl groups, as we will discuss later in this section. By proper comparison of results obtained with different samples, we can investigate the interactions between GLY and different minerals in an original approach. From **Table 6** we note that GLY adsorbed on forsterite and pyrite has a shorter half-life compared with GLY adsorbed on antigorite and spinel; in particular, GLY adsorbed on spinel did not show degradation in most of its bands during the 7-h irradiation session. **Table 9** reports results relative to bands that showed degradation in all samples. In detail, we considered three bands of three different types of functional groups that showed degradation in all samples. (1) For wagging and twisting mode of $-CH_2^-$, located around 1,311/1,333 cm^{-1}, we found comparable shorter half-life times between forsterite and pyrite, while spinel turned out to be the most effective mineral in slowing down the reaction involving GLY. (2) Looking at the symmetric stretching of $-COO^-$ group, we found again the longest half-life time when GLY is adsorbed on spinel. (3) for bending of NH_3^+, we could not make any considerations due to larger uncertainties. Generally speaking, we can say that the whole set of samples can be divided into two subgroups: the first formed by spinel and antigorite with lower values of photodissociation parameters; the second group formed by forsterite and pyrite with higher values. The fact that pyrite and forsterite show a higher catalytic effect could be linked to typical high reactivity of iron-bearing minerals (Fornaro et al., 2018b). Spinel and antigorite did not show any significant catalytic effect. The serpentine minerals, such as antigorites, are characterized by high surface areas and lamellar structure with optimal interlayer sites for adsorption and shielding of organic molecules. These findings agree with the UV irradiation studies of amino acids adsorbed on various minerals under Martian-like conditions carried out by dos Santos et al. (2016), revealing that phyllosilicates have a greater tendency to preserve GLY degradation with respect to other minerals. The lower catalytic effect of antigorite with respect to forsterite was also observed in recent works carried out in our laboratory using different classes of prebiotic molecules (Fornaro et al., 2018a; Potenti et al., 2018). The catalytic activity of some minerals may be related to a proximity effect, i.e., their ability to increase the local concentration of molecules through adsorption onto the mineral surfaces and, consequentially, the probability of molecular self-association and chemical reactions. Moreover, molecular adsorption may take place with a configuration that facilitates interactions between reactive functional groups of molecules close to each other on the surface. According to

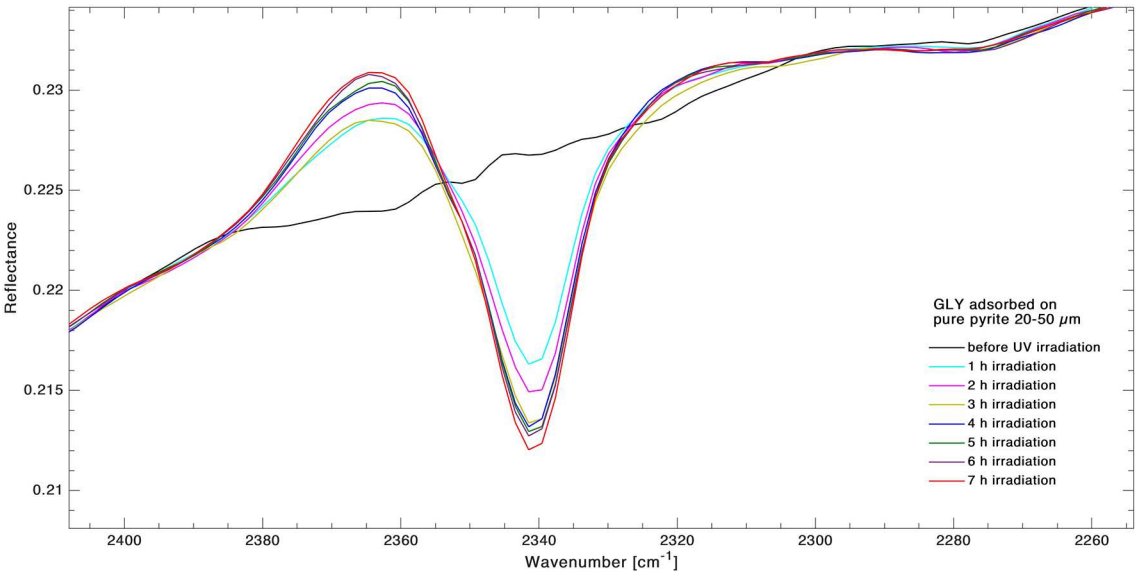

FIGURE 6 | Superimposition of infrared spectra of GLY adsorbed on pyrite for forming band at 2,340 cm^{-1} during 7 h of UV irradiation. Spectra were collected *in situ* at 1-h intervals to monitor the kinetics of degradation in real time. The growing band area of CO_2 band is clearly visible.

TABLE 9 | Comparison of half-life of GLY adsorbed on forsterite, antigorite, spinel, and pyrite for three common bands.

Mode	Half-life time $t_{\frac{1}{2}}$ [*min*]			
	Forsterite	**Antigorite**	**Spinel**	**Pyrite**
$twCH_2$ and ωCH_2	47 ± 6	67 ± 9	146 ± 49	32 ± 3
$\nu_s COO^-$	58 ± 9	46 ± 12	130 ± 34	73 ± 30
δNH_3^+	25 ± 16	109 ± 68	78 ± 18	147 ± 53

previous works, antigorite seems to have lower catalytic effect than forsterite (Fornaro et al., 2018a; Potenti et al., 2018) or pyrite. We also observed lower catalytic properties in the case of spinel.

Formation of new peaks was observed when we irradiated GLY on pyrite (**Figure 6**). The newly formed peak is associated with carbon dioxide, specifically with asymmetric stretching of CO_2. Ehrenfreund et al. (2001) suggest that the photodissociation process of GLY (reported in the text that follows in its non-zwitterionic form) starts with the separation of the carboxyl group:

$$H_2NCH_2COOH + h\nu \rightarrow H_2NCH_2 + COOH$$

According to Guan et al. (2010), after hydrogen atom transfer between COOH and H_2NCH_2 radicals, the formation of CO_2 and methylamine (CH_3NH_2) is quite straightforward, being followed by the formation of HCN. Since GLY in our samples is in its zwitterionic form, the aforementioned transfer has already occurred and so CO_2 can form directly. The persistence of a long period of CO_2 bands in laboratory conditions can be due to an entrapment in deeper layers of the sample from which they cannot easily escape. Only bands attributable to CO_2 were revealed in the spectra, neither CH_3NH_2 nor HCN bands were visible. The CO_2 band formation has also been observed in other laboratory experiments with GLY and pyrite irradiated with the same lamp in vacuum under pressure of 10^{-6} mbar (data not shown), confirming that the appearance of this band CO_2 band is linked with GLY dissociation.

Observation of degradation of GLY bands and formation of new peaks in about 7 h of irradiation under ambient temperature suggest that short-time photoprocessing active in the equatorial region of Mars close to noon can affect strongly GLY fate. Rovers such as Exomars 2022 and Mars 2020 will perform *in situ* analysis, drilling the subsurface for sample collection. Our work shows how the presence of organics such as GLY can be seriously affected according to irradiation history along the drill depth. We could also think about pioneering experiments in which the samples extracted from subsurface are exposed to UV radiation to study Mars photo-reactions directly to infer the effects of possible resurfacing processes that can affect exposed biomolecules extracted from the subsoil. On the other hand, this may also suggest that if this adsorbed GLY is exposed to UV for a short time and then is covered later on by another layer that protects from UV, the molecule that is preserved would be different, altered, and would show different bands from the original one.

To conclude our discussion, as inferred from our work, hydrated phyllosilicates such as serpentine show the lowest catalytic photodegradation activity among the tested minerals, especially if compared with the other minerals such as pyrite and forsterite. These results, while confirming the resistance of glycine against UV irradiation, give us new hints in seeking organic material in space, helping interpretation of ExoMars 2022 data in searching for organics on Mars.

CONCLUSIONS

In our work we analyzed the UV irradiation of pure GLY and adsorbed on space-relevant minerals that are abundant in a wide range of environments across the Solar System: the serpentine antigorite, olivine forsterite, oxide mineral spinel, and iron–sulfide mineral pyrite. Among organic relevant molecules we chose glycine [GLY], the simplest amino acid, one of the 20 included in terrestrial biology, and already found in meteorites and comets.

After sample preparation, we were able to assign GLY molecular peak positions on molecule-mineral samples from the previous literature. We generally observed a decrease of band intensity and peak shifts with respect to pure GLY as a consequence of adsorption.

We performed UV irradiation of several hours following in real time the kinetics of degradation to evaluate parameters such as cross sections and half-life of GLY adsorbed on selected minerals. We found differences in degradation processes depending on the mineral used as adsorbent. In our study, we highlight a lower efficiency of antigorite and spinel in catalyzing GLY photoreaction compared with forsterite and pyrite. The half-life changes between the four GLY-mineral samples from a factor of about 2 up to a factor of about 4 times, as reported in our work. From σ values estimated in our laboratory conditions, it is possible to derive the half-life values experienced under the Martian UV flux [estimated by Patel et al. (2002) as 1.4×10^{15} photons s^{-1} cm^{-2} in the 190–325 nm spectral range] by using the same relations between σ, β, and Φ_{tot}. In particular, we found that GLY adsorbed on pyrite has a half-life of about 40 h; in comparison this value can be doubled in the presence of antigorite, with a half-life of 80 Martian hours. Instruments such as MOMA on board ExoMars 2022 will need this kind of information to increase the probability of detection of organic material before taking the decision to move forward in the analysis with single-use ovens (Goesmann et al., 2017). Generally speaking, in the present and future searches for biomarkers on Mars and in the Solar System, mineral composition will be an important factor to be considered for positive detection.

DATA AVAILABILITY STATEMENT

The datasets generated for this study are available on request to the corresponding author.

AUTHOR CONTRIBUTIONS

GP and TF prepared and characterized all the samples. GP and SP carried out irradiation experiments. GP, JB, and MC performed data analysis. All authors assisted in interpretation and contributed to the writing of the manuscript.

FUNDING

The authors wish to thank the Italian Space Agency for co-funding the Life in Space project (ASI N. 2019-3-U.0).

SUPPLEMENTARY MATERIAL

The Supplementary Material for this article can be found online at: https://www.frontiersin.org/articles/10.3389/fspas.2020.00018/full#supplementary-material

Supplementary Figure A1 | Infrared spectrum of pure milled and dried GLY in range 8,000–400 cm^{-1}.

Supplementary Figure A2 | Infrared spectrum of for sterite (grain dimension 20–50 μm), either pure or GLY-spiked, in the range 4,000–400 cm^{-1}.

Supplementary Figure A3 | Infrared spectrum of antigorite (grain dimension 20–50 μm), either pure or GLY-spiked, in the range 4,000–400 cm^{-1}.

Supplementary Figure A4 | Infrared spectrum of spinel (grain dimension 20–50 μm), either pure or GLY-spiked, in the range 4,000–400 cm^{-1}.

Supplementary Figure A5 | Infrared spectrum of pyrite (grain dimension 20–50 μm), either pure or GLY-spiked, in the range 4,000–400 cm^{-1}.

REFERENCES

Agee, C. B., Wilson, N. V., McCubbin, F. M., Ziegler, K., Polyak, V. J., Sharp, Z. D., et al. (2013). Unique meteorite from early amazonian Mars: water-rich basaltic breccia Northwest Africa 7034. *Science*. 339, 780–785. doi: 10.1126/science.1228858

Altwegg, K., Balsiger, H., Bar-Nun, A., Berthelier, J.-J., Bieler, A., Bochsler, P., et al. (2016). Prebiotic chemicals—amino acid and phosphorus—in the coma of comet 67P/Churyumov-Gerasimenko. *Sci. Adv*. 2:e1600285. doi: 10.1126/sciadv.1600285

Bach, W., Paulick, H., Garrido, C. J., Ildefonse, B., Meurer, W. P., and Humphris, S. E. (2006). Unraveling the sequence of serpentinization reactions: petrography, mineral chemistry, and petrophysics of serpentinites from MAR 15°N (ODP Leg 209, Site 1274). *Geophys. Res. Lett*. 33:L13306. doi: 10.1029/2006GL025681

Barbier, B., Chabin, A., Chaput, D., and Brack, A. (1998). Photochemical processing of amino acids in Earth orbit. *Planet. Space Sci.* 46, 391–398. doi: 10.1016/S0032-0633(97)00150-5

Barbier, B., Henin, O., Boillot, F., Chabin, A., Chaput, D., and Brack, A. (2002). Exposure of amino acids and derivatives in the Earth orbit. *Planet. Space Sci.* 50, 353–359. doi: 10.1016/S0032-0633(02)00010-7

Bernal, J. D. (1951). *The Physical Basis of Life*. London: Routledge & Kegan Paul.

Bernstein, M. P., Dworkin, J. P., Sandford, S. A., Cooper, G. W., and Allamandola, L. J. (2002). Racemic amino acids from the ultraviolet photolysis of interstellar ice analogues. *Nature.* 416, 401–403. doi: 10.1038/416401a

Bjärnborg, K., and Schmitz, B. (2013). Large spinel grains in a CM chondrite (Acfer 331): implications for reconstructions of ancient meteorite fluxes. *Meteorit. Planet. Sci.* 48, 180–194. doi: 10.1111/maps.12050

Brownlee, D., Tsou, P., Aléon, J., Alexander, C. M. O.'D., Araki, T., Bajt, S., et al. (2006). Comet 81P/Wild 2 under a microscope. *Science.* 314, 1711–1716. doi: 10.1126/science.1135840

Brucato, J. R., Strazzulla, G., Baratta, G. A., Rotundi, A., and Colangeli, L. (2006). Cryogenic synthesis of molecules of astrobiological interest: catalytic role of cosmic dust analogues. *Orig Life Evol. Biosph.* 36, 451–457. doi: 10.1007/s11084-006-9050-5

Carter, J., Poulet, F., Bibring, J.-P., Mangold, N., Murchie, S., Langevin, Y., et al. (2009). "Phyllosilicates and Other Hydrated Minerals on Mars: Global Distribution as Seen by MEx/OMEGA," in *Proceedings of the 40th Lunar and Planetary Science Conference* (Woodlands, TX).

Chevrier, V., and Mathé P. E. (2007). Mineralogy and evolution of the surface of Mars: a review. *Planet. Space Sci.* 55, 289–314. doi: 10.1016/j.pss.2006.05.039

de La Cruz-López, A., del Ángel-Meraz, E., Colín-García, M., Ramos-Bernal, S., Negrón-Mendoza, A., and Heredia, A. (2017). Ultraviolet irradiation of glycine in presence of pyrite as a model of chemical evolution: an experimental and molecular modelling approach. *Int. J. Astrobiol.* 16, 1–7. doi: 10.1017/S1473550416000161

dos Santos, R., Patel, M., Cuadros, J., and Martins, Z. (2016). Influence of mineralogy on the preservation of amino acids under simulated Mars conditions. *Icarus* 277, 342–353. doi: 10.1016/j.icarus.2016.05.029

Ehlmann, B. L., Mustard, J. F., Clark, R. N., Swayze, G. A., and Murchie, S. L. (2011). Evidence for low-grade metamorphism, hydrothermal alteration, and diagenesis on Mars from phyllosilicate mineral assemblages. *Clays Clay Mineral*. 59, 359–377. doi: 10.1346/CCMN.2011.0590402

Ehlmann, B. L., Mustard, J. F., and Murchie, S. L. (2010). Geologic setting of serpentine deposit on Mars. *Geophys. Res. Lett.* 37:L0620. doi: 10.1029/2010GL042596

Ehlmann, B. L., Mustard, J. F., Swayze, G. A., Clark, R. N., Bishop, J. L., Poulet, F., et al. (2009). Identification of hydrated silicate minerals on Mars using MRO-CRISM: geologic context near Nili Fossae and implications for aqueous alteration. *J. Geophys. Res.* 114. doi: 10.1029/2009JE003339

Ehrenfreund, P., Bernstein, M. P., Dworkin, J. P., Sandford, S. A., and Allamandola, L. J. (2001). The photostability of amino acids in space. *Astrophys. J.* 550:L95. doi: 10.1086/319491

Ertem, G. (2004). Montmorillonite, oligonucleotides, RNA and origin of life. *Orig. Life Evol. Biosph.* 34, 549–570. doi: 10.1023/B:ORIG.0000043130.49790.a7

Fornaro, T., Boosman, A., Brucato, J. R., ten Kate, I. L., Siljeström, S., Poggiali, G., et al. (2018a). UV irradiation of biomarkers adsorbed on minerals under Martian-like conditions: hints for life detection on Mars. *Icarus* 313, 38–60. doi: 10.1016/j.icarus.2018.05.001

Fornaro, T., Brucato, J. R., Branciamore, S., and Pucci, A. (2013a). Adsorption of nucleic acid bases on magnesium oxide (MgO). *Int. J. Astrobiol.* 12, 78–86. doi: 10.1017/S1473550412000444

Fornaro, T., Brucato, J. R., Pace, E., Cestelli Guidi, M., Branciamore, S., and Pucci, A. (2013b). Infrared spectral investigations of UV irradiated nucleobases adsorbed on mineral surfaces. *Icarus* 226, 1068–1085. doi: 10.1016/j.icarus.2013.07.024

Fornaro, T., Steele, A., and Brucato, J. R. (2018b). Catalytic/protective properties of martian minerals and implications for possible origin of life on Mars. *Life*. 8:56. doi: 10.3390/life8040056

Galvez-Martinez, S., Escamilla-Roa, E., Zorzano, M.-P., and Mateo-Marti, E. (2019). Defects on a pyrite(100) surface produce chemical evolution of glycine under inert conditions: experimental and theoretical approaches. *Phys. Chem. Chem. Phys.* 21. doi: 10.1039/C9CP03577J

Glavin, D. P., and Bada, J. L. (2004). Survival of amino acids in micrometeorites during atmospheric entry. *Astrobiology* 1, 259–269. doi: 10.1089/15311070152757456

Glavin, D. P., Dworkin, J. P., and Sandford, S. A. (2008). Detection of cometary amines in samples returned by Stardust. *Meteorit. Planet. Sci.* 43, 399–413. doi: 10.1111/j.1945-5100.2008.tb00629.x

Goesmann, F., Brinckerhoff, W. B., Raulin, F., Goetz, W., Danell, R. M., Getty, S. A., et al. (2017). The Mars Organic Molecule Analyzer (MOMA) instrument: characterization of organic material in martian sediments. *Astrobiology* 17, 655–685. doi: 10.1089/ast.2016.1551

Guan, Y. Y., Fray, N., Coll, P., Macari, F., Chaput, D., Raulin, F., et al. (2010). UVolution: compared photochemistry of prebiotic organic compounds in low Earth orbit and in the laboratory. *Planet. Space Sci.* 58, 1327–1346. doi: 10.1016/j.pss.2010.05.017

Hadraoui, K., Cottin, H., Ivanovski, S. L., Zapf, P., Altwegg, K., Benilan, Y., et al. (2019). Distributed glycine in comet 67P/Churyumov-Gerasimenko. *Astronomy Astrophys.* 630:A32. doi: 10.1051/0004-6361/201935018

Hazen, R. M., and Sverjensky, D. A. (2010). Mineral surfaces, geochemical complexities, and the origins of life. *Cold Spring Harb. Perspect. Biol.* 2:a002162. doi: 10.1101/cshperspect.a002162

Holtom, P. D., Bennett, C. J., Osamura, Y., Mason, N. J., and Kaiser, R. I. (2005). A combined experimental and theoretical study on the formation of the amino acid glycine (NH2CH2COOH) and its isomer (CH3NHCOOH) in extraterrestrial ices. *Astrophys. J.* 626:940. doi: 10.1086/430106

Johnson, P. V., Hodyss, R., Chernow, V. F., Lipscomb, D. M., and Goguen, J. D. (2012). Ultraviolet photolysis of amino acids on the surface of icy solar system bodies. *Icarus* 221, 800–805. doi: 10.1016/j.icarus.2012.09.005

Kvenvolden, K., Lawless, J., Pering, K., Peterson, E., Flores, J., Ponnamperuma, C., et al. (1970). Evidence for extraterrestrial amino-acids and hydrocarbons in the murchison meteorite. *Nature* 228, 923–926. doi: 10.1038/228923a0

Lambert, J. F., Sakhno, Y., Battistella, A., Ribetto, B., Mezzetti, A., Georgelin, T., et al. (2017). "Could mineral surfaces have oriented amino acid polymerization towards useful products?," in *XVIIIth International Conference on the Origin of Life, Proceedings of the Conference* (San Diego, CA).

Luther, A., Brandsch, R., and von Kiedrowski, G. (1998). Surface-promoted replication and exponential amplification of DNA analogues. *Nature* 396, 245–248. doi: 10.1038/24343

Messenger, S., Keller, L. P., and Lauretta, D. S. (2005). Supernova olivine from cometary dust. *Science* 309, 737–741. doi: 10.1126/science.1109602

Moriarty, D., Hibbitts, C. A., Lisse, C. M., Dyar, M. D., Harlow, G., Ebel, D., et al. (2010). "Near-Far IR spectra of sulfide minerals relevant to comets,"in *41st Lunar and Planetary Science Conference* (Woodlands, TX), 2447

Muñoz Caro, G. M., Mateo-Martí E., and Martínez-Frías, J. (2006). Near-UV transmittance of basalt dust as an analog of the martian regolith: implications for sensor calibration and astrobiology. *Sensors* 6, 688–696. doi: 10.3390/s6060688

Muñoz Caro, G. M., Meierhenrich, U. J., Schutte, W. A., Barbier, B., Arcones Segovia, A., Rosenbauer, H., et al. (2002). Amino acids from ultraviolet irradiation of interstellar ice analogues. *Nature* 416, 403–406. doi: 10.1038/416403a

Noblet, A., Stalport, F., Guan, Y. Y., Poch, O., Coll, P., Szopa, C., et al. (2012). The PROCESS experiment: amino and carboxylic acids under Mars-like surface UV radiation conditions in low-earth orbit. *Astrobiology* 12, 436–444. doi: 10.1089/ast.2011.0756

Orzechowska, G. E., Goguen, J. D., Johnson, P. V., Tsapin, A., and Kanik, I. (2007). Ultraviolet photolysis of amino acids in a 100 K water ice matrix: application to the outer solar system bodies. *Icarus* 187, 584–591. doi: 10.1016/j.icarus.2006.10.018

Patel, M. R., Zarnecki, J. C., and Catling, D. C. (2002). Ultraviolet radiation on the surface of Mars and the Beagle 2 UV sensor. *Planet. Space Sci.* 50, 915–927. doi: 10.1016/S0032-0633(02)00067-3

Peeters, Z., Botta, O., Charnley, S. B., Ruiterkamp, R., and Ehrenfreund, P. (2003). The astrobiology of nucleobases. *Astrophys. J.* 593:L129. doi: 10.1086/378346

Pilling, S., Mendes, L. A., Bordalo, V., Guaman, C. F., Ponciano, C. R., and da Silveira, E. F. (2013). The influence of crystallinity degree on the glycine decomposition induced by 1 MeV proton bombardment in space analog conditions. *Astrobiology* 13, 79–91. doi: 10.1089/ast.2012.0877

Poch, O., Kaci, S., Stalport, F., Szopa, C., and Coll, P. (2014). Laboratory insights into the chemical and kinetic evolution of several organic molecules under simulated Mars surface UV radiation conditions. *Icarus* 242, 50–63. doi: 10.1016/j.icarus.2014.07.014

Poch, O., Noblet, A., Stalport, F., Correia, J. J., Grand, N., Szopa, C., et al. (2013). Chemical evolution of organic molecules under Mars-like UV radiation conditions simulated in the laboratory with the "Mars organic molecule irradiation and evolution" (MOMIE) setup. *Planet. Space Sci.* 85, 188–197. doi: 10.1016/j.pss.2013.06.013

Poteet, C. A., Megeath, S. T., Watson, D. M., Calvet, N., Remming, I. S., McClure, M. K., et al. (2011). A spitzer infrared spectrograph detection of crystalline silicates in a protostellar envelope. *Astrophys. J. Lett.* 733:L32. doi: 10.1088/2041-8205/733/2/L32

Potenti, S., Manini, P., Fornaro, T., Poggiali, G., Crescenzi, O., Napolitano, A., et al. (2018). Solid state photochemistry of hydroxylated naphthalenes on minerals: probing polycyclic aromatic hydrocarbon transformation pathways under astrochemically-relevant conditions. *ACS Earth Space Chem.* 2, 977–1000. doi: 10.1021/acsearthspacechem.8b00060

Rivkin, A. S., and Emery, J. P. (2010). Detection of ice and organics on an asteroidal surface. *Nature* 464, 1322–1323. doi: 10.1038/nature09028

Rosado, M. T., Duarte, M. L. T. S., and Fausto, R. (1998). Vibrational spectra of acid and alkaline glycine salts. *Vib. Spectrosc.* 16, 35–54. doi: 10.1016/S0924-2031(97)00050-7

Saidel, L. J., Goldfarb, A., and Waldman, S. (1952). The absorption spectra of amino acids in the region two hundred to two hundred and thirty millimicrons. *J. Biol. Chem.* 197, 285–91.

Schoonen, M., Smirnov, A., and Cohn, C. (2004). A perspective on the role of minerals in prebiotic synthesis. *AMBIO* 33, 539–51. doi: 10.1579/0044-7447-33.8.539

Snyder, L. E., Lovas, F. J., Hollis, J. M., Friedel, D. N., Jewell, P. R., Remijan, A., et al. (2005). A rigorous attempt to verify interstellar glycine. *Astrophys. J.* 619:914. doi: 10.1086/426677

Steel, I. M. (1989). "Forsterite in CI meteorites and interplanetary dust: minor elements and comparison with other meteorite types,"in *Abstracts of the Lunar and Planetary Science Conference, Vol. 20* (Houston, TX), 1054.

ten Kate, I. L., Garry, J. R. C., Peeters, Z., Quinn, R., Foing, B., and Ehrenfreund, P. (2005). Amino acid photostability on the Martian surface. *Meteorit. Planet. Sci.* 40, 1185–1193. doi: 10.1111/j.1945-5100.2005.tb00183.x

Vago, J., Witasse, O., Svedhem, H., Baglioni, P., Haldemann, A., Gianfiglio, G., et al. (2015). ESA ExoMars program: the next step in exploring Mars. *Solar Syst. Res.* 49, 518–528. doi: 10.1134/S0038094615070199

Viviano-Beck, C. E., Seelos, F. P., Murchie, S. L., Kahn, E. G., Seelos, K. D., Taylor, H. W., et al. (2014). Revised CRISM spectral parameters and summary products based on the currently detected mineral diversity on Mars. *J. Geophys. Res. Planets* 119, 1403–1431. doi: 10.1002/2014JE004627

Weinbruch, S., Palme, H., and Spettel, B. (2010). Refractory forsterite in primitive meteorites: condensates from the solar nebula? *Meteorit. Planet. Sci.* 35, 161–171. doi: 10.1111/j.1945-5100.2000.tb01983.x

Williford, K. H., Farley, K. A., Stack, K. M., Allwood, A. C., Beaty, D., Beegle, L. W., et al. (2018). "The NASA Mars 2020. rover mission and the search for extraterrestrial life," in: *From Habitability to Life on Mars.* eds N. Cabrol and E. Grim (Amsterdam: Elseivier), 275–308. doi: 10.1016/B978-0-12-809935-3.00010-4

Woon, D. E. (2002). Pathways to glycine and other amino acids in ultraviolet-irradiated astrophysical ices determined via quantum chemical modeling. *Astrophys. J.* 571:L177. doi: 10.1086/341227

Yu, Y., and Gee, J. (2005). Spinel in Martian meteorite SaU 008: implications for Martian magnetism. *Earth Planet. Sci. Lett.* 232, 287–294. doi: 10.1016/j.epsl.2004.12.015

Conflict of Interest: The authors declare that the research was conducted in the absence of any commercial or financial relationships that could be construed as a potential conflict of interest.